Electron tomography reveals a flared morphology on growing microtubule ends

Johanna L. Höög[1,2,3,*], Stephen M. Huisman[1,4], Zsofia Sebö-Lemke[1], Linda Sandblad[1], J. Richard McIntosh[3], Claude Antony[1,‡] and Damian Brunner[1,4,‡]

[1]European Molecular Biology Laboratories, Cell Biology and Biophysics Program, D-69117 Heidelberg, Germany
[2]Sir William Dunn School of Pathology, University of Oxford, Oxford OX1 3RE, UK
[3]The Boulder Laboratory of 3D EM of Cells, Cellular and Developmental Biology, University of Colorado, Boulder, CO 80309, USA
[4]Institute of Molecular Life Sciences, University of Zürich, 8057, Switzerland

*Author for correspondence (johanna.hoog@path.ox.ac.uk)
‡These authors contributed equally to this work

Accepted 26 October 2010
Journal of Cell Science 124, 693-698

doi:10.1242/jcs.072967

Summary

Microtubules (MTs) exhibit dynamic instability, alternating between phases of growth and shortening, mostly at their uncapped plus ends. Based on results from cryo-electron microscopy it was proposed that growing MTs display mainly curved sheets and blunt ends; during depolymerisation curled 'ramshorns' predominate. Observations of MTs in mitotic cells have suggested that the situation in vivo differs from that in vitro, but so far, a clear comparison between in vivo and in vitro results has not been possible because MT end structures could not be correlated directly with the dynamic state of that particular MT. Here we combine light microscopy and electron tomography (ET) to show that growing MT plus ends in the fission yeast *Schizosaccharomyces pombe* display predominantly a flared morphology. This indicates that MT polymerisation in vivo and in vitro can follow different paths.

Key words: Microtubule polymerisation, Plus ends, Electron tomography, *Schizosaccharomyces pombe*

Introduction

Microtubules (MTs) are essential cytoskeletal elements involved in crucial cellular functions such as cell division, intracellular transport and the control of cell shape. They undergo slow growth or rapid shortening, a trait termed dynamic instability (Mitchison and Kirschner, 1984). This behaviour is mostly confined to the MT plus end in vivo, because minus ends are commonly stabilised by the γ-tubulin ring complex (γ-TURC) (Moritz et al., 1995; O'Toole et al., 1999; O'Toole et al., 2003). The γ-TURC nucleates MTs and forms a cap on their minus end (Keating and Borisy, 2000; Moritz et al., 2000; Wiese and Zheng, 2000).

MT growth has been studied in vitro by negative stain and cryo-EM. In these studies, 60–70% of the growing plus ends are blunt (Simon and Salmon, 1990; Mandelkow et al., 1991; Vitre et al., 2008). Curved sheets of multiple protofilaments extending from growing MT ends are also present (Simon and Salmon, 1990; Chretien et al., 1995; Vitre et al., 2008); sheets are more prevalent in high tubulin concentrations where the MTs grow more rapidly (Chretien et al., 1995; Vitre et al., 2008).

It is plausible, however, that MT growth in vivo is different from that in vitro. In vitro microtubules have a variable number of protofilaments (McEwen and Edelstein, 1977) and are formed in the absence of MT-associated proteins (MAPs). In the semi-in-vivo *Xenopus* egg extract system, the ends of growing MTs were mostly long sheets (53%); 23% of ends were blunt and 23% were curled (Arnal et al., 2000).

In mitotic spindles of the amoeba *Dictyostelium discoideum*, cross-sections of MT plus ends appeared as C-shapes, implying a sheet-like extension of the MT wall (McIntosh et al., 1985). Electron tomography of high-pressure frozen and plastic-embedded dividing plant cells showed up to 46% of MTs ending in curved sheets (Austin et al., 2005). In a cryo-electron tomography study of mouse embryonic fibroblasts, only 35% of the MT plus ends were sheets; 26% of the ends were blunt and 40% displayed curved protofilaments (Koning et al., 2008). However, sheet-like MT plus ends are rare in yeasts and human cells. Here, a majority of MT ends are flared, meaning that most or all of their tubulin protofilaments splay out from the MT axis (O'Toole et al., 1999; O'Toole et al., 2003; Höög et al., 2007; McIntosh et al., 2008). In an effort to understand the diversity seen in these reports, we have studied growing MT ends in *Schizosaccharomyces pombe* after release from a MT-depolymerising drug, using electron tomography to answer the question how MTs grow inside a cell.

Results and Discussion

Microtubules re-grow rapidly after MBC washout

The fission yeast interphase MT cytoskeleton consists of three to six cytoplasmic bundles that are approximately aligned with the long cell axis (Fig. 1A). MT minus ends are found mainly near the cell mid-plane, where they form a region of anti-parallel MT overlap. From this region, the MT plus ends grow toward the two poles of the cylindrical cells (La Carbona et al., 2006; Sawin and Tran, 2006). To analyse the structure of growing MT plus ends, we used large-scale electron tomography of fission yeast cells containing MTs that were all growing after washout of the fungicide, methyl benzimidazol-2-yl-carbamate (MBC), the MT-depolymerising drug of choice in *S. pombe* (Sawin and Snaith, 2004). MBC inhibits MT polymerisation by binding to free tubulin rather than actively depolymerising MTs (supplementary material Fig. S1). Real-time fluorescence microscopy of MBC-treated cells expressing GFP-tagged α-tubulin (GFP–α-tubulin) confirmed the presence of one or two short, MBC-resistant MT 'stubs', as previously described (Sawin and Snaith, 2004) (Fig. 1A). Ultra-structural investigation using electron tomography (ET) showed

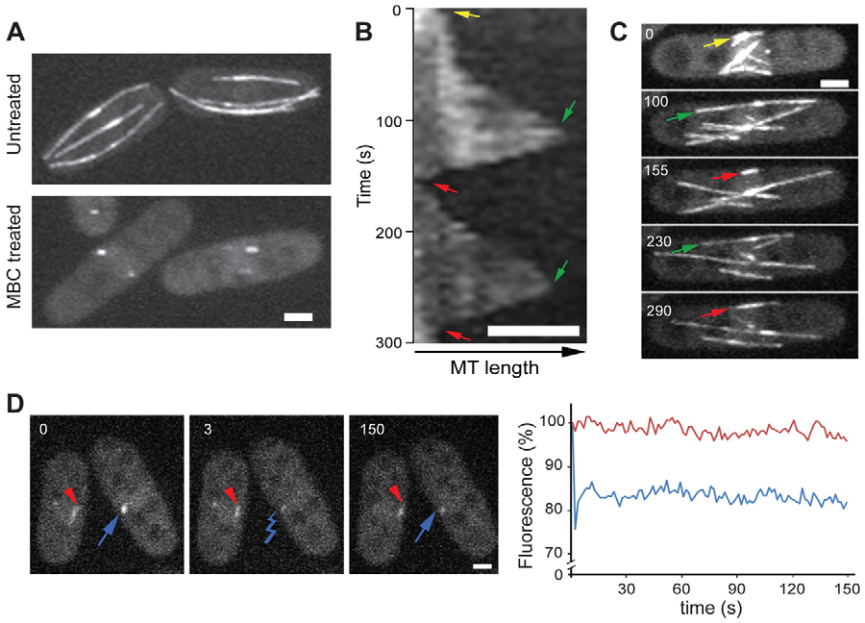

Fig. 1. Dynamics of regrowing MTs and MT 'stubs'. (**A**) Live *S. pombe* cells expressing GFP–α-tubulin before and after MBC addition. (**B**) Kymograph of the bundle highlighted in C. An initial lag phase (yellow arrow), was followed by a period of polymerisation (green arrows) that was not faster than polymerisation measured in untreated bundles. This growth was followed by MT depolymerisation (red arrows). (**C**) MT bundle (GFP–α-tubulin) regrowth after MBC wash-out (time 0). (**D**) Fluorescence recovery after photobleaching experiment (FRAP) shows that MT stubs have little or no turn-over. Blue arrow and line indicate bleached stub; red arrowhead and line indicate control stub. Scale bars: 2 µm.

that the 3D architecture of these stubs was similar to the overlap region in untreated cells (supplementary material Fig. S2, Movies 1 and 2). The preferred MT–MT distance and MT–MT angle in treated cells were comparable with those found in the untreated cells; however the number of MTs in each bundle was greater.

Using live-cell imaging, we observed a burst of MT growth immediately after MBC washout (Fig. 1B,C). MTs started growing at both ends of the residual stubs. In addition, several new MT arrays appeared in the cell centre from which MTs grew in opposite directions. Interestingly, the MT polymerisation rate did not increase compared with untreated cells (2.2±0.8 µm/minute; mean ± s.d. (n=48) and 2.6±0.8 µm/minute (n=51), respectively; Fig. 1B). The simultaneous growth of all MT bundles lasted for approximately 2 minutes, after which the first depolymerising MT bundles were observed. Within 5 minutes, wild-type MT distribution and dynamicity were re-established (Fig. 1C; supplementary material Movie 3), shifting proportions from 100% growing MT bundles to 80% growing MT bundles, as normally found in these cells (Höög et al., 2007).

We investigated the dynamics of MTs in the drug-resistant stubs of MBC-treated cells. Cells expressing GFP–α-tubulin were treated with MBC for 15 minutes or more, then photobleached and the recovery of fluorescence was monitored. We observed minimal or no fluorescence recovery (n=10; Fig. 1D) during 2.5 minutes in MBC-treated cells, whereas interphase MTs in untreated cells turned over approximately every 2 minutes. This indicates that the stubs consist of hyper-stabilised MTs.

Growing microtubule ends are mostly flared

To describe the morphologies of growing MT plus ends, we reconstructed EM tomograms from cells in early interphase (6–7 µm in length; Fig. 2A). Tomograms were made from cryoimmobilised cells in three different conditions: untreated, MBC-treated and 90 seconds after MBC washout. All cells were subsequently fixed by freeze-substitution (Höög and Antony, 2007). The MTs in MBC-released cells were considerably shorter (0.17±0.23 µm; n=64) than in untreated cells [1.64±1.43 µm, n=70 (Höög et al., 2007)]. They ranged from 30 nm to 1.1 µm in length and were arranged in bundles around the nucleus (Fig. 2B,C and supplementary material Movie 4). Notably, intranuclear MT bundles were found both during MBC treatment and after drug release (supplementary material Fig. S3 and Movie 5).

We then identified the MT ends and categorised them, based on their 3D appearance. We distinguished between ends that were capped, blunt, extended by curved tubulin sheets, or displayed curled or flared protofilaments (Fig. 2B,D). MT ends with curling protofilaments ('ramshorns') in vitro are generally thought to be depolymerising (Simon and Salmon, 1990; Mandelkow et al., 1991; Chretien et al., 1995; Tran et al., 1997a; Müller-Reichert et al., 1998; Arnal et al., 2000; Zovko et al., 2008). Flared protofilaments were 17.7±7.5 nm long (n=58), and extended from the MT in a kinked or curved fashion.

We next determined MT polarity by identifying capped MT ends, which represent minus ends that are protected by the γ-TURC (O'Toole et al., 1999; O'Toole et al., 2003). The other end of these MTs are almost certainly growing plus ends, given the MBC wash-out. However, in MBC-treated cells 31% of MTs were open at both ends, suggesting they have uncapped dynamic minus ends (n=19 out of 61 MTs). Such uncapped MTs were observed in 21% (n=12/74 MTs) of the MBC-depleted cells, and in 26% (n=12/56 MTs) of MTs in untreated control cells (supplementary material Table S2). MTs lacking a capped end were considered in our statistics on plus-end structure only if both ends showed the same morphology. Examining cells after MBC washout, we found that 90% of the identifiable growing MT plus ends had a flared morphology; this included 11% that were flared at both ends (Fig. 2E). Many short MTs had flared plus ends (Fig. 2F). Our results show that in fission yeast, the growing MT plus ends are mostly flared. Because of the large fraction of flared ends in the hyper-stable MTs, detectable during MBC treatment (Fig. 2E), MTs probably display flared ends during several dynamic states, not only during growth.

Sheets are unusual microtubule end structures in vivo

In this study, we examined a total of 526 MT plus-end and minus-end structures, of which only seven (1.3%) were sheets

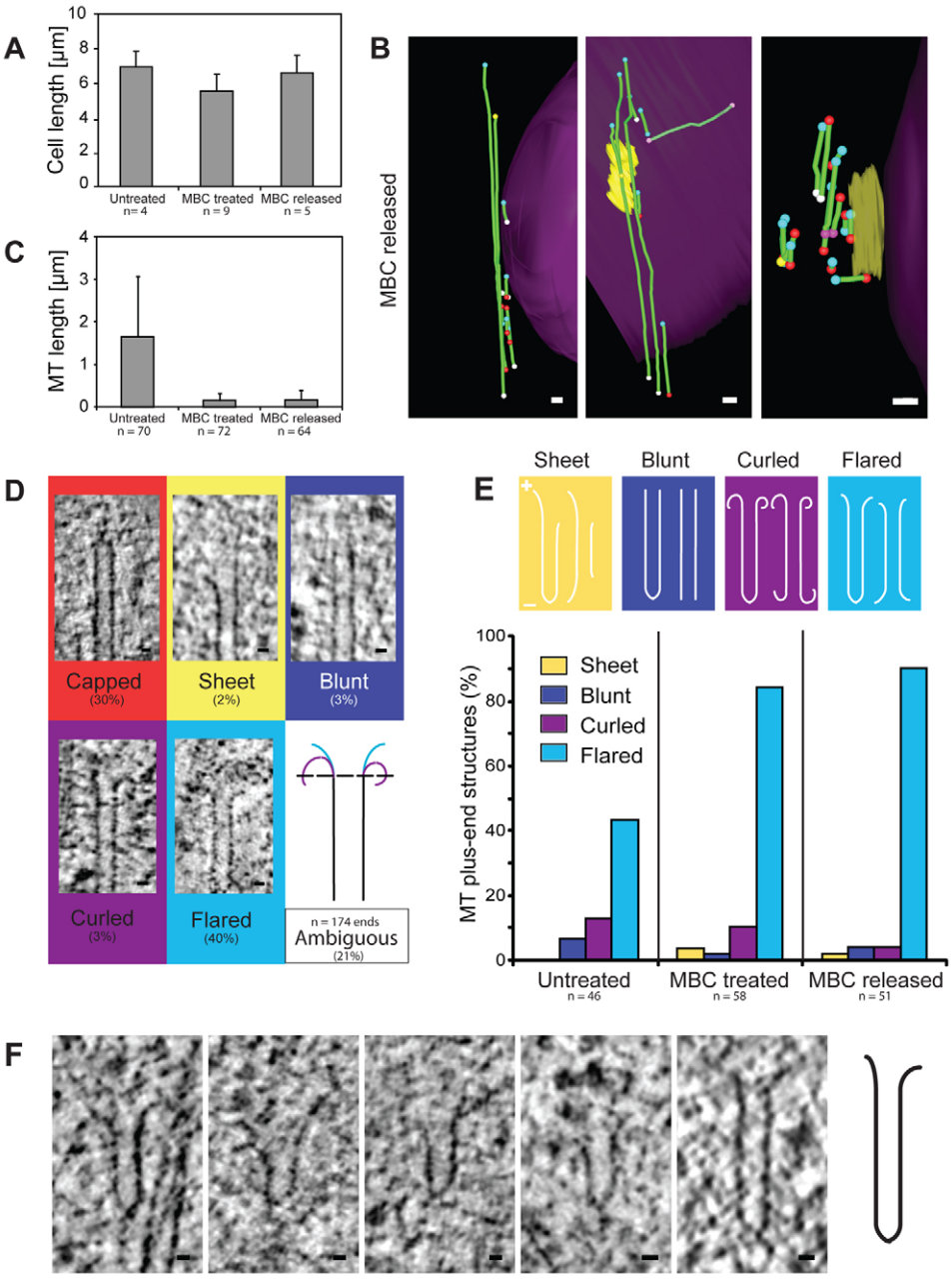

Fig. 2. Most regrowing MT plus ends are flared. (**A**) We used cell length to select cells in early G2 for tomography reconstructions (mean ± s.d.). (**B**) Tomographic 3D models of MT bundle architecture 90 seconds after MBC wash-out. MTs (green filaments) have flared (turquoise balls), capped (red), curled (purple), sheeted (yellow) or ambiguous (white) ends. The SPB (centrosome equivalent) is visible in yellow, sitting on the nuclear envelope (pink). (**C**) Individual MT lengths were short during MBC treatment and remained shorter than in the wild type after release. (**D**) A gallery of MT end structures, percentage of the total population of ends (*n*=174) in MBC-released cells, and a cartoon illustrating how the flared ends (turquoise lines) were separated from the curled ends (purple lines). Ends are curled if the protofilament end meets a line positioned where the protofilaments leave the main MT axis (dashed line). (**E**) Plus ends were defined as the end opposite to a capped end, or when MTs had two similar ends, e.g. flared/flared. MTs with two open ends, e.g. flared/blunt, were considered of unknown polarity. The graph shows the percentage of plus-end morphologies found in untreated, MBC-treated and MBC-released cells. Flared plus ends predominate on growing MTs. (**F**) A gallery of short MTs with one capped end and one flared end. Scale bars: 50 nm (B), 10 nm (D,F).

(supplementary material Table S3). When the 51 plus ends of growing MTs were studied, only one (2%) was found to be a sheet. In comparison, no sheets were found on known MT plus ends (*n*=46) in untreated cells, and two (3%; *n*=58) of the plus ends in MBC-treated cells were sheets. Thus, sheets are the rarest of the MT end structures found, and a population of mostly growing MT plus ends does not notably increase this fraction. Moreover, the sheets we did find were structurally different from those found in *Xenopus* extract. In this study, sheets were 63±20 nm long (*n*=7), whereas sheets in the previous study were ~440 nm long on average (Arnal et al., 2000).

The nature of blunt microtubule ends

Previous studies have seen blunt MT ends as a sub-population of growing ends (Simon and Salmon, 1990; Arnal et al., 2000). It has also been proposed that blunt ends are a metastable intermediate between growing and shrinking phases (Tran et al., 1997b; Vitre et al., 2008). In our study, blunt plus ends are found with similar frequencies in both MBC-treated (2% of MT plus ends; Fig. 2E) and MBC-released (4%) cells; thus their dynamic state in vivo remains inconclusive.

New model of microtubule growth

Although it is clear that MAP activity is used to control global MT organisation and behaviour, the extent to which it also creates structural variety is not known. In particular, the impact of MAPs on structure at dynamic MT plus ends has not been studied. The main reason for this lack of knowledge is the difficulty of studying MT plus ends in vivo and in 3D. In addition, it is usually impossible to assign a specific structure to the dynamic state of a particular MT end. Here we have used ET in combination with the depletion of a MT depolymerising drug to unambiguously

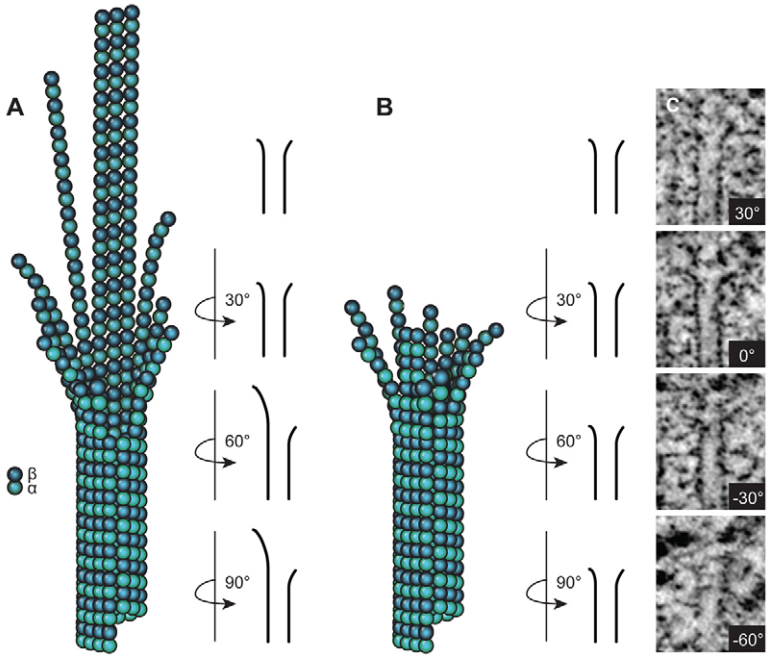

Fig. 3. Growing MT plus ends are mostly funnel-like structures. (**A**) Cartoon of a short sheet structure, as well as a line drawing representative of what would be seen in different orientations in a tomographic reconstruction of such a sheet. (**B**) A new funnel-like growing MT structure, which would be seen as a flared end imaged from all angles. (**C**) 4-nm-thick tomographic slices showing the same MT over a range of 30° angles, with a flared end in each view, showing that it is a structure as visualised in B.

describe the morphology of growing MT plus ends in fission yeast cells. We found that growing MT ends mostly consist of short flares.

In principle, this flared appearance could reflect two structures: one where the protofilaments form a single curved sheet structure (Fig. 3A) and another where the individual protofilaments form a funnel with little or loose lateral interaction (Fig. 3B). However, a sheet only appears flared if viewed perpendicular, or close to perpendicular, to the sheet surface; a funnel flares out at any viewing angle. Because we viewed MT ends from all available angles and still observed mostly flared ends (Fig. 3C), we can conclude that in the fission yeast cells, MT plus ends appear to grow by the closing of a funnel-like structure.

Similar flared MT plus-ends were documented in two recent publications, although the dynamic state of those MT ends was not always clear (Koning et al., 2008) or they were visualised during depolymerisation (McIntosh et al., 2008). Flared MT end structures in vivo differ considerably from the curved sheet or blunt end structures that dominate in vitro and in *Xenopus* egg extracts (Kirschner et al., 1975; Simon and Salmon, 1990; Chretien et al., 1995; Arnal et al., 2000). Flared MT ends were also seen in cryo-EM of growing MTs in in vitro preparations (Chretien et al., 1995). Although it cannot be fully excluded that the large proportion of sheets in these previous studies is an experimental artefact caused during sample blotting or by interaction of the MTs with the EM grid, it is conceivable that differences in the structure of growing MT plus ends reflect differences in the nature of MT polymerisation in different cell types with differing MAP composition and tubulin concentration.

In vivo, MT assembly might occur in at least two different ways depending on the cellular conditions (Arnal et al., 2000) (this study). However, these two growth modes do not need to be fundamentally different. Any model for MT elongation requires the longitudinal addition of tubulin subunits to protofilaments and their coalescence to form a tube by lateral interaction. What differs is merely the timing of lateral protofilament binding. If protofilaments immediately interact with their neighbours during elongation, the natural curvature of the protofilaments will bend any sheet that forms slightly outward, away from the tube. In this case, the protofilament sheet can flip into a tube conformation only at a distance from the growing end. In the second method of growth presented here, the closing of flared ends does not require such flipping. Here the protofilaments first elongate and then successively ‘zip up’ with their neighbours. Therefore, our data seem to argue against a closure mechanism centred at the seam of MTs and favour a model of MT elongation by random lateral protofilament connection at the MT end.

One can envision MAPs that monitor correct lattice geometry during MT growth. A possible candidate for such a regulator of MT closure is mal3p, the *S. pombe* EB1, which binds in between protofilaments (Sandblad et al., 2006; des Georges et al., 2008). In vitro studies have reported that sites of selective mal3p/EB1 binding to growing MT plus ends persist for 8 seconds, independently of MT polymerisation rates (Bieling et al., 2007; Dixit et al., 2009). In our in vivo study, 8 seconds correspond to 300 nm of protofilament elongation, which is considerably longer than the flared protofilaments at MT ends (<20 nm). This comparison suggests that mal3 binding sites are not restricted solely to the flared protofilaments themselves, but extend from the protofilaments into the adjacent region of the closed MT lattice.

In addition to the concerted action of MAPs, tubulin concentration is another possible way to influence the decision on whether to grow with a sheet or a funnel-like end structure. In vitro, MT growth accelerates with increasing tubulin concentration. If protofilament elongation outpaces the binding of MAPs that inhibit lateral protofilament fusion, then protofilaments can again efficiently interact laterally and form curved sheets. Interestingly, the tubulin concentration is higher in *Xenopus* egg extracts than it is in yeasts, which could explain the differences found at growing MT plus ends in the two systems (Gard and Kirschner, 1987).

By presenting good evidence for a second type of growing MT end structure that dominates in fission yeast cells and is distinct from the previously suggested ‘closing sheet model’, this study promotes a view in which multiple modes of MT elongation exist

in vivo. It is now important to repeat our experiments using other cell types to determine whether the variety in MT growth methods found in vivo is created by the concerted MAP actions of that particular species.

Materials and Methods

Fluorescence microscopy

Logarithmically growing cells in minimal media (EMM2), with appropriate supplements, thiamine and with or without 25 μg/ml MBC, were used for imaging using a PerkinElmer Ultraview (E)RS spinning disc confocal microscopes (488 nm laser line of an Argon ion laser for imaging and bleaching) or an Apo 100×/1.30 NA oil objective or an epifluorescent Axiovert 200 M microscope (Zeiss; Plan-Apo100×/1.4 NA objective).

For FRAP experiments h-lys1+::nmt1p:GFP:atb2 ura4-D18 cells were incubated with MBC for 15 minutes before photobleaching. Stacks of three slices were taken every 1.5 seconds and maximum projected with ImageJ.

For MBC-release experiments, h-sad1-dsRed::leu2+ lys1+::nmt1p:GFP:atb2 nup85:GFP::KAN^{R} leu1-32 ura4-D18 cells (lab collection) were incubated with MBC for 15 minutes before release. Imaging started within 20 seconds of washing out the MBC. A stack of nine slices was taken every 5 seconds and maximum projected with ImageJ. Kymographs of individual MTs were made using an Image J plugin (J. Rietdorf, FMI, Basel, Switzerland and A. Seitz, EMBL, Heidelberg, Germany).

Specimen preparation for electron microscopy

Cultures of logarithmically growing WT fission yeasts were treated with 25 μg/ml methyl 2-benzimidazolecarbamate (MBC) for 15 minutes. To gain samples of MBC-treated as well as drug wash-out samples, cells were filtered and either (1) cryo-immobilised directly by high-pressure freezing, using a BAL-TEC HPM 010, or (2) washed with MBC-free medium before immediate cryo-immobilisation. Samples were then freeze substituted, embedded in Lowicryl and cut in 250-nm-thick sections, as described (Höög and Antony, 2007).

Electron tomography

For tomography, the grids were placed in a high tilt holder (Model 2020; Fischione Instruments; Corporate Circle, PA). Low-magnification maps of serial sections were made using the Navigator function in SerialEM software (Mastronarde, 2005). Digital images (Gatan Ultrascan 890 or 895, pixel size 1.5 nm) were taken every 1–1.25° over a ±65° range on a FEI Tecnai TF20 electron microscope. Variations of montaged single-axis tilt series (14,500×), or single frame dual axis tilt series (14,500–20,000×) were collected. Approximately 65 tomograms were made of each sample, allowing the reconstruction of partial volumes from nine MBC-treated cells and five cells after drug release.

Modelling and analysis of tomographic data

Tomograms were displayed as slices one voxel thick, modelled and analysed using the IMOD software package (Kremer et al., 1996). MTs were tracked using the 'slicer' tool. The morphology of MT ends was examined in several planes, all of which contained the MT axis and were marked with colour-coded scattered points to distinguish between capped, flared, sheet, curled, blunt and ambiguous ends (Höög et al., 2007). A projection of the 3D model was displayed using 3dmod. MT lengths were extracted using the IMODINFO program.

Filtration experiment

Increasing amounts of MBC (0–333 μM) were mixed with 45 μM purified porcine tubulin (a generous gift from E. Karsenti, EMBL, Heidelberg, Germany). The mixture was filtrated through Ultrafree-MC centrifugal filter column units (model Biomax-10; Millipore, Germany) retaining proteins >10 kDa. The amount of MBC in elute was measured by its specific absorption at 284 nm by a nano-drop spectrophotometer (NanoDrop^{TM} 1000; Thermo Scientific).

We thank all members of our labs for helpful discussions and constant support; H. Schwartz for his help with cryoimmobilisation; A. Kotecha for help with calculating tomograms; K. Gull, T. Surrey and I. Arnal for helpful discussions. J.L.H. was first supported by a Marie Curie Early Stage Research Training Fellowship of the European Community's Sixth Framework Programme (FP6) under contract number MEST-CT-2004-504640, then EMBO postdoctoral fellowship and Sir Henry Wellcome postdoctoral fellowship (from the Wellcome Trust). S.M.H. is supported by Deutsche Forschungsgemeinschaft (DFG) and a Marie Curie Intra European fellowship within the 7th European Community Framework Programme. This work was also supported by National Institutes of Health Biotechnology Resources grant RR000592 to Andreas Hoenger. Deposited in PMC for release after 6 months.

Supplementary material available online at
http://jcs.biologists.org/cgi/content/full/124/5/693/DC1

References

Arnal, I., Karsenti, E. and Hyman, A. A. (2000). Structural transitions at microtubule ends correlate with their dynamic properties in Xenopus egg extracts. *J. Cell Biol.* **149**, 767-774.

Austin, J. R., II, Segui-Simarro, J. M. and Staehelin, L. A. (2005). Quantitative analysis of changes in spatial distribution and plus-end geometry of microtubules involved in plant-cell cytokinesis. *J. Cell Sci.* **118**, 3895-3903.

Bieling, P., Laan, L., Schek, H., Munteanu, E. L., Sandblad, L., Dogterom, M., Brunner, D. and Surrey, T. (2007). Reconstitution of a microtubule plus-end tracking system in vitro. *Nature* **450**, 1100-1105.

Chretien, D., Fuller, S. D. and Karsenti, E. (1995). Structure of growing microtubule ends: two-dimensional sheets close into tubes at variable rates. *J. Cell Biol.* **129**, 1311-1328.

des Georges, A., Katsuki, M., Drummond, D. R., Osei, M., Cross, R. A. and Amos, L. A. (2008). Mal3, the Schizosaccharomyces pombe homolog of EB1, changes the microtubule lattice. *Nat. Struct. Mol. Biol.* **15**, 1102-1108.

Dixit, R., Barnett, B., Lazarus, J. E., Tokito, M., Goldman, Y. E. and Holzbaur, E. L. (2009). Microtubule plus-end tracking by CLIP-170 requires EB1. *Proc. Natl. Acad. Sci. USA* **106**, 492-497.

Gard, D. L. and Kirschner, M. W. (1987). Microtubule assembly in cytoplasmic extracts of Xenopus oocytes and eggs. *J. Cell Biol.* **105**, 2191-2201.

Höög, J. L. and Antony, C. (2007). Whole-cell investigation of microtubule cytoskeleton architecture by electron tomography. *Methods Cell Biol.* **79**, 145-167.

Höög, J. L., Schwartz, C., Noon, A. T., O'Toole, E. T., Mastronarde, D. N., McIntosh, J. R. and Antony, C. (2007). Organization of interphase microtubules in fission yeast analyzed by electron tomography. *Dev. Cell* **12**, 349-361.

Keating, T. J. and Borisy, G. G. (2000). Immunostructural evidence for the template mechanism of microtubule nucleation. *Nat. Cell Biol.* **2**, 352-357.

Kirschner, M. W., Honig, L. S. and Williams, R. C. (1975). Quantitative electron microscopy of microtubule assembly in vitro. *J. Mol. Biol.* **99**, 263-276.

Koning, R. I., Zovko, S., Barcena, M., Oostergetel, G. T., Koerten, H. K., Galjart, N., Koster, A. J. and Mieke Mommaas, A. (2008). Cryo electron tomography of vitrified fibroblasts: microtubule plus ends in situ. *J. Struct. Biol.* **161**, 459-468.

Kremer, J. R., Mastronarde, D. N. and McIntosh, J. R. (1996). Computer visualization of three-dimensional image data using IMOD. *J. Struct. Biol.* **116**, 71-76.

La Carbona, S., Le Goff, C. and Le Goff, X. (2006). Fission yeast cytoskeletons and cell polarity factors: connecting at the cortex. *Biol. Cell* **98**, 619-631.

Mandelkow, E. M., Mandelkow, E. and Milligan, R. A. (1991). Microtubule dynamics and microtubule caps: a time-resolved cryo-electron microscopy study. *J. Cell Biol.* **114**, 977-991.

Mastronarde, D. N. (2005). Automated electron microscope tomography using robust prediction of specimen movements. *J. Struct. Biol.* **152**, 36-51.

McDonald, K. L., O'Toole, E. T., Mastronarde, D. N. and McIntosh, J. R. (1992). Kinetochore microtubules in PTK cells. *J. Cell Biol.* **118**, 369-383.

McEwen, B. and Edelstein, S. J. (1977). Evidence for a mixed lattice in microtubules reassembled in vitro. *J. Mol. Biol.* **139**, 123-143.

McIntosh, J. R., Roos, U. P., Neighbors, B. and McDonald, K. L. (1985). Architecture of the microtubule component of mitotic spindles from Dictyostelium discoideum. *J. Cell Sci.* **75**, 93-129.

McIntosh, J. R., Grishchuk, E. L., Morphew, M. K., Efremov, A. K., Zhudenkov, K., Volkov, V. A., Cheeseman, I. M., Desai, A., Mastronarde, D. N. and Ataullakhanov, F. I. (2008). Fibrils connect microtubule tips with kinetochores: a mechanism to couple tubulin dynamics to chromosome motion. *Cell* **135**, 322-333.

Mitchison, T. and Kirschner, M. (1984). Dynamic instability of microtubule growth. *Nature* **312**, 237-242.

Moritz, M., Braunfeld, M. B., Sedat, J. W., Alberts, B. and Agard, D. A. (1995). Microtubule nucleation by gamma-tubulin-containing rings in the centrosome. *Nature* **378**, 638-640.

Moritz, M., Braunfeld, M. B., Guenebaut, V., Heuser, J. and Agard, D. A. (2000). Structure of the gamma-tubulin ring complex: a template for microtubule nucleation. *Nat. Cell Biol.* **2**, 365-370.

Müller-Reichert, T., Chretien, D., Severin, F. and Hyman, A. A. (1998). Structural changes at microtubule ends accompanying GTP hydrolysis: information from a slowly hydrolyzable analogue of GTP, guanylyl (alpha,beta)methylenediphosphonate. *Proc. Natl. Acad. Sci. USA* **95**, 3661-3666.

O'Toole, E. T., Winey, M. and McIntosh, J. R. (1999). High-voltage electron tomography of spindle pole bodies and early mitotic spindles in the yeast Saccharomyces cerevisiae. *Mol. Biol. Cell* **10**, 2017-2031.

O'Toole, E. T., McDonald, K. L., Mäntler, J., McIntosh, J. R., Hyman, A. A. and Müller-Reichert, T. (2003). Morphologically distinct microtubule ends in the mitotic centrosome of Caenorhabditis elegans. *J. Cell Biol.* **163**, 451-456.

Sandblad, L., Busch, K. E., Tittmann, P., Gross, H., Brunner, D. and Hoenger, A. (2006). The Schizosaccharomyces pombe EB1 homolog Mal3p binds and stabilizes the microtubule lattice seam. *Cell* **127**, 1415-1424.

Sawin, K. E. and Snaith, H. A. (2004). Role of microtubules and tea1p in establishment and maintenance of fission yeast cell polarity. *J. Cell Sci.* **117**, 689-700.

Sawin, K. E. and Tran, P. T. (2006). Cytoplasmic microtubule organization in fission yeast. *Yeast* **23**, 1001-1014.

Simon, J. R. and Salmon, E. D. (1990). The structure of microtubule ends during the elongation and shortening phases of dynamic instability examined by negative-stain electron microscopy. *J. Cell Sci.* **96**, 571-582.

Tran, P. T., Joshi, P. and Salmon, E. D. (1997a). How tubulin subunits are lost from the shortening ends of microtubules. *J. Struct. Biol.* **118**, 107-118.

Tran, P. T., Walker, R. A. and Salmon, E. D. (1997b). A metastable intermediate state of microtubule dynamic instability that differs significantly between plus and minus ends. *J. Cell Biol.* **138**, 105-117.

Vitre, B., Coquelle, F. M., Heichette, C., Garnier, C., Chretien, D. and Arnal, I. (2008). EB1 regulates microtubule dynamics and tubulin sheet closure in vitro. *Nat. Cell Biol.* **10**, 415-421.

Wiese, C. and Zheng, Y. (2000). A new function for the gamma-tubulin ring complex as a microtubule minus-end cap. *Nat. Cell Biol.* **2**, 358-364.

Zovko, S., Abrahams, J. P., Koster, A. J., Galjart, N. and Mommaas, A. M. (2008). Microtubule plus-end conformations and dynamics in the periphery of interphase mouse fibroblasts. *Mol Biol. Cell*. **19**, 3138-3146.